

Single-Crystal-to-Single-Crystal Post-Synthetic Modifications of Three-Dimensional LOFs (Ln = Gd, Eu): a Way to Modulate their Luminescence and Thermometric Properties.

Jacopo De Bellis[‡], Luca Bellucci,[§] Gregorio Bottaro,^{§†*} Luca Labella,^{‡†*} Fabio Marchetti,[‡] Simona Samaritani,[‡] Daniela Belli Dell'Amico,[‡] and Lidia Armelao^{§†}

[‡]*Dipartimento di Chimica e Chimica Industriale and CIRCC, Università di Pisa, via Giuseppe Moruzzi 13, I-56124*

[§]*Dipartimento di Scienze Chimiche, Università di Padova, via Marzolo 1, I-35131*

[†]*CNR ICMATE and INSTM, Dipartimento di Scienze Chimiche, Università di Padova, via Marzolo 1, I-35131*

Contents

Figure S1. FTIR spectra of **1** (blue) and **2** (red).

Figure S2. PXRD patterns of **1** (blue) and **2** (red) compared with the calculated pattern for **2** (black).

Figure S3. Powder X-ray of **3** (blue) and **4** (red) compared with the calculated pattern for **3** (black).

Figure S4. FTIR spectra of **3** (blue) and **4** (red).

Figure S5. PXRD patterns of **5** (blue) and **6** (red) compared with the calculated pattern for **5** (black).

Figure S6. FTIR spectra of **5** (blue) and **6** (red).

Figure S7. The lanthanide coordination polyhedron a) in **2**, which the labels refer to, in **3** and in Gd1 of **5** and b) in Gd2 of **5**.

Figure S8. Diffuse reflectance spectra of compounds **1**, **3**, and **5**.

Figure S9. a) Excitation spectra of compounds **2**, **4**, and **6**; b) expansion of the 350-450 nm of PLE spectra reported in a) $\lambda_{em} = 614$ nm. The vertical dotted lines in panel b) evidence the position of the onset of LMCT bands (Figure 9) for **4** (light blue) and **6** (green).

Figure S10. a), b), and c) emission spectra of compounds **1**, **3**, and **5** at 298 K (dashed lines) and 83 K (full lines) temperature. d) Time delayed emission spectra of compounds **1**, **3**, and **5** recorded at 83 K after 40 μ s.

Figure S11. Superimposition of the coordination sphere for: a) **2** and **3**, b) **2** and Gd1 of **5**, c) **2** and Gd2 of **5**.

Figure S12. Temperature-dependent emission spectra of compounds **2**, **4**, and **6** in the 83 \div 303 K temperature range.

Figure S13. Thermal cycling of compounds a) **2**, b) **4**, and c) **6**.

Figure S14. Temperature dependence of the Δ parameter in **4** and **6**. The colored dots represent the experimental points while the black line represents the data of the best fit ($R^2=0.999$) of the Mott-Seitz model (MS) involving two non-radiative recombination channels.

Figure S15. IR spectra of compounds **2**, **4**, and **6**.

Table 1. Bond distances (\AA) around the metal listed following the corresponding edges of coordination polyhedra.

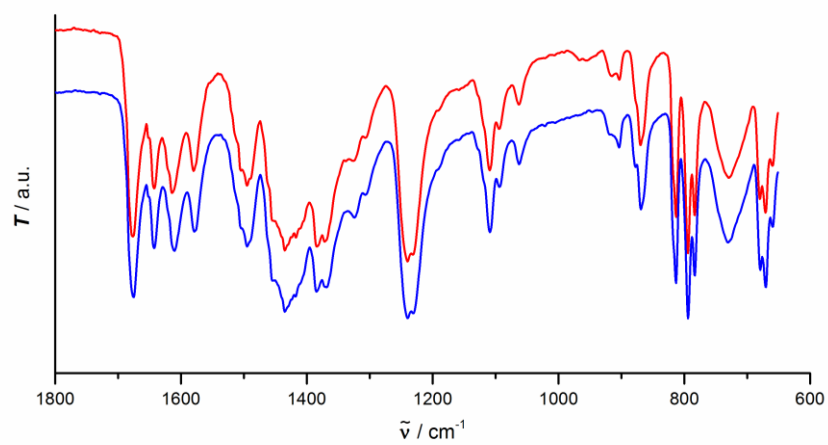


Figure S1. FTIR spectra of **1** (blue) and **2** (red).

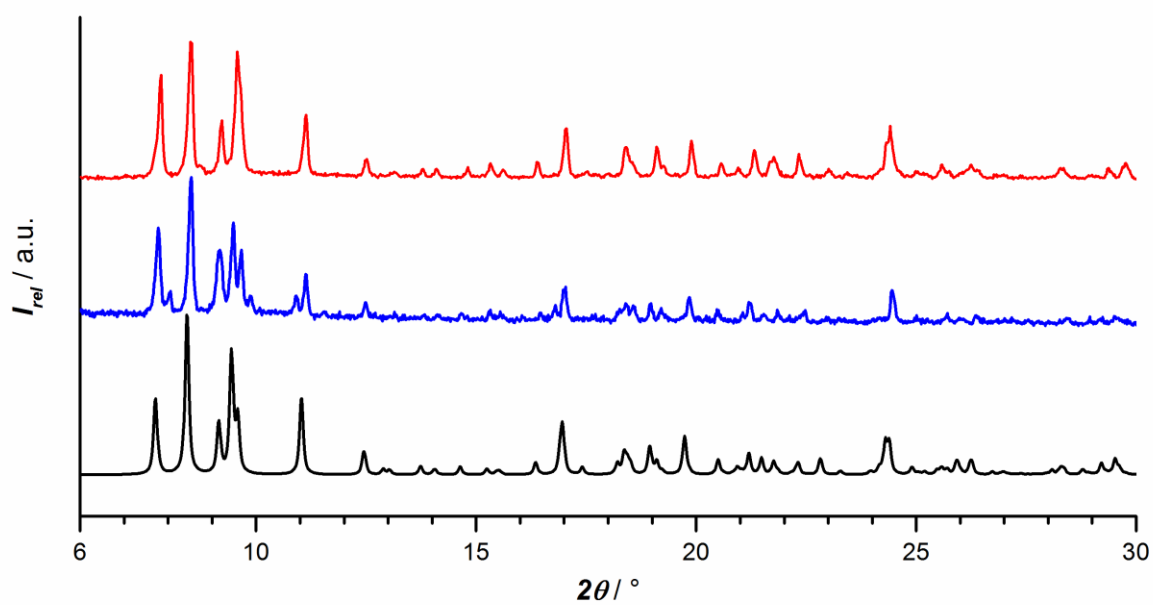


Figure S2. PXRD patterns of **1** (blue) and **2** (red) compared with the calculated pattern for **2** (black).

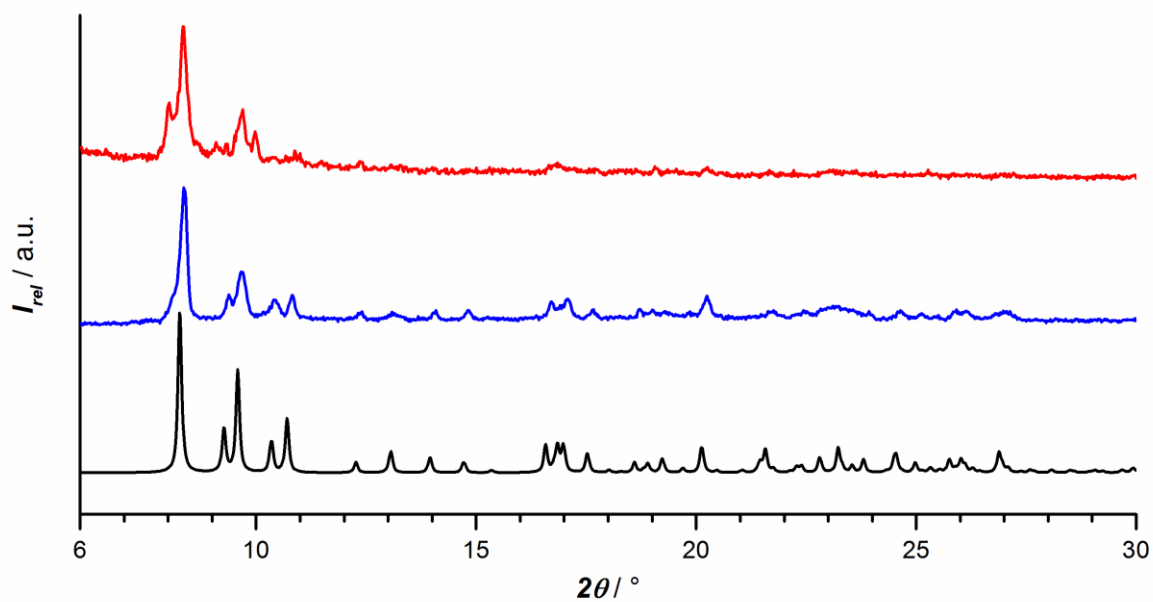


Figure S3. Powder X-ray of **3** (blue) and **4** (red) compared with the calculated pattern for **3** (black).

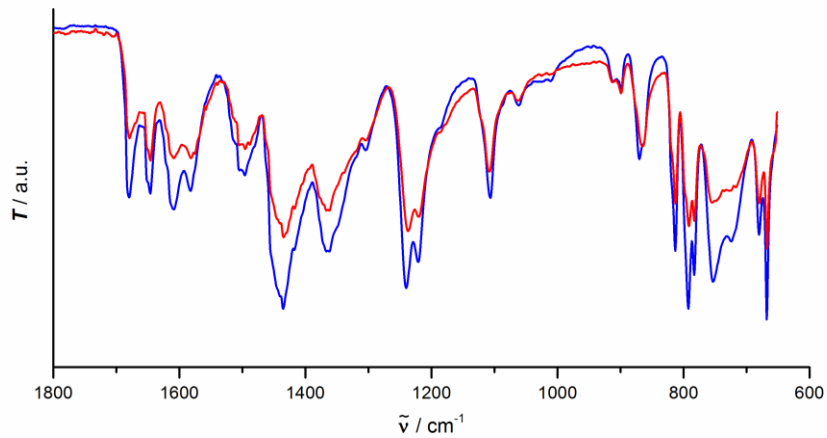


Figure S4. FTIR spectra of **3** (blue) and **4** (red).

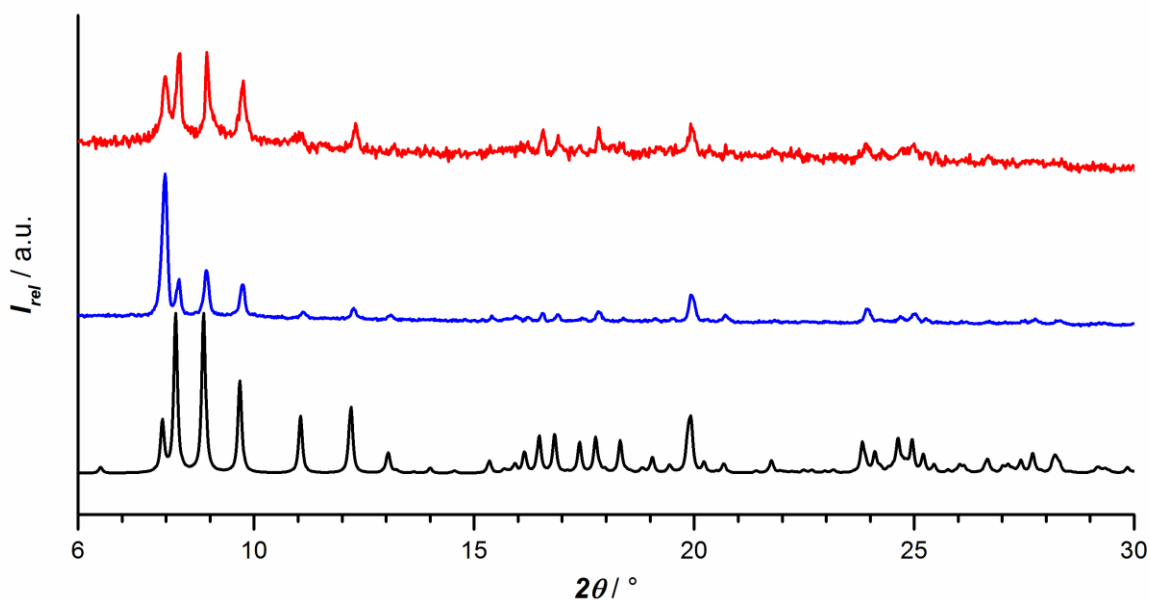


Figure S5. PXRD patterns of **5** (blue) and **6** (red) compared with the calculated pattern for **5** (black).

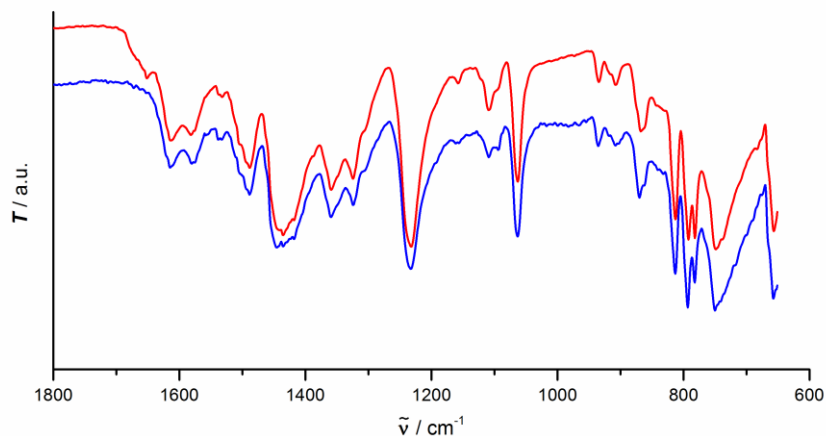


Figure S6. FTIR spectra of **5** (blue) and **6** (red).

Coordination geometry of lanthanide centres.

The crystal structures of the compounds treated in this work are related to that of **1**, of which they share the topology. Due to the distortions of the scaffold caused by the different filling of the cavities, some of the bridging carboxylate oxygens come more or less close to each of the metals in the pair. The coordination geometry around each lanthanide is square antiprismatic. The ninth Ln...O distance is in all cases markedly longer than the other eight.

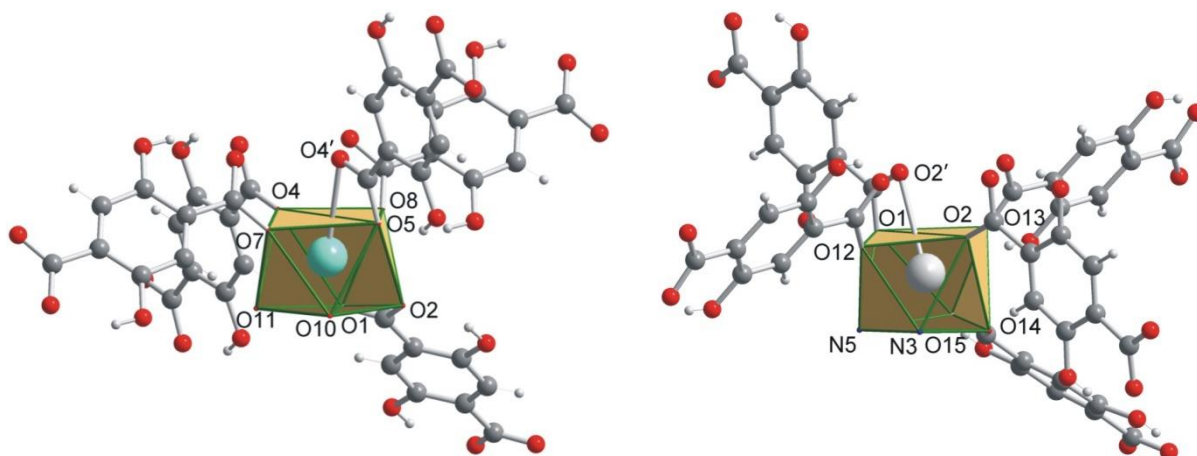


Figure S7. The lanthanide coordination polyhedron a) in **2**, which the labels refer to, in **3** and in Gd1 of **5** and b) in Gd2 of **5**.

Table 1. Bond distances (Å) around the metal listed following the corresponding edges of coordination polyhedra.

	2	3	5
Eu1–O1	2.436(2)	Gd1–O2	2.450(5)
Eu1–O2	2.5599(18)	Gd1–O1	2.526(5)
Eu1–O4	2.3468(18)	Gd1–O4	2.334(5)
Eu1...O4'	2.9143(19)	Gd1...O4'	2.9729(3)
Eu1–O5	2.4153(18)	Gd1–O5	2.426(5)
Eu1–O7	2.3676(16)	Gd1–O7	2.378(5)
Eu1–O8	2.4067(16)	Gd1–O8	2.406(5)
Eu1–O10	2.4241(19)	Gd1–O11	2.421(6)
Eu1–O11	2.450(5)	Gd1–O10	2.372(6)
		Gd1–O18	2.524(3)
		Gd1–O19	2.472(2)
		Gd1–O5	2.316(3)
		Gd1...O5'	3.066(3)
		Gd1–O6	2.425(2)
		Gd1–O8	2.364(2)
		Gd1–O9	2.391(2)
		Gd1–N1	2.538(3)
		Gd1–O7	2.428(3)
		Gd2–O15	2.566(3)
		Gd2–O14	2.429(3)
		Gd2–O1	2.420(3)
		Gd2...O2'	2.929(3)
		Gd2–O2	2.332(2)
		Gd2–O12	2.355(2)
		Gd2–O13	2.412(2)
		Gd2–N3	2.547(3)
		Gd2–N5	2.511(3)

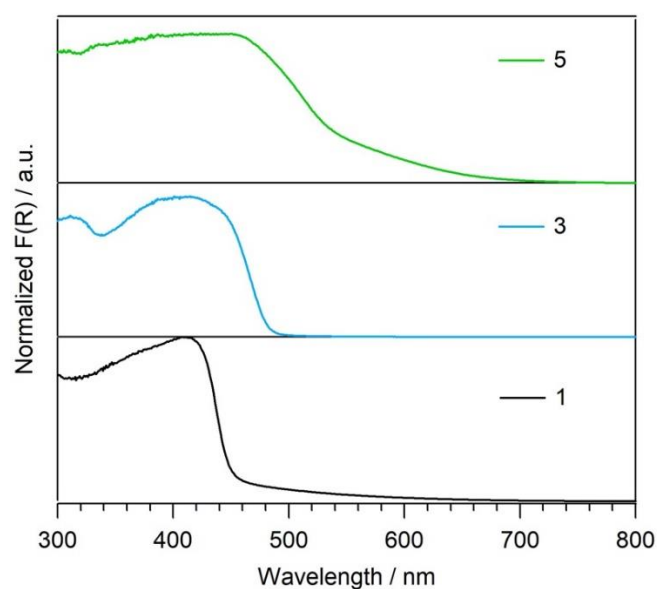


Figure S8. Diffuse reflectance spectra of compounds **1**, **3**, and **5**.

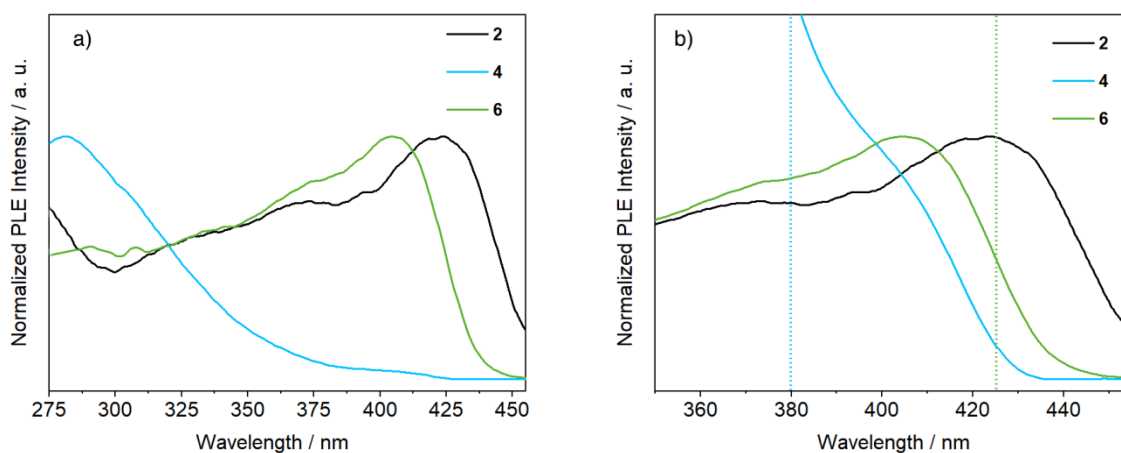


Figure S9. a) Excitation spectra of compounds **2**, **4**, and **6**; b) expansion of the 350-450 nm of PLE spectra reported in a) $\lambda_{em} = 614$ nm. The vertical dotted lines in panel b) evidence the position of the onset of LMCT bands (Figure 9) for **4** (light blue) and **6** (green).

PLE spectrum of **4** (Figure S9a) is quite different from those of **2** and **6** being characterized by an intense signal centred at *ca.* 280 nm and by a long tail up 400-420 nm. The spectrum of **2** shows a slope change below *ca.* 300 nm that could be the tail of a band with the maximum centred deeper in the UV-region. This evidence suggests that the PLE spectra of this family of Eu^{3+} -based MOFs can have bands in the UV, but their positions can not be directly correlated with MOF structure. When the spectra are normalized to better highlight the region around 400 nm (Figure S9b), we can observe a shoulder in the spectrum of **4**. A feature that closely resembles the shape of the curves of **2** and **6** in this region, but with an onset blue-shifted respect to both those of **2** and **6**. The PLE spectra of the three MOFs share some features, but the position and relative intensity of the bands are affected by the presence of DMF, CHCl_3 and Im. We have evidence that low energy LMCT transitions influence the shape of the absorption spectra in the visible. It is worth to be highlighted that they can be only qualitatively revealed by the arithmetic subtraction of the europium and gadolinium absorption spectra, but nothing can be said about possible: *i*) overlaps with ligand centred transitions, and *ii*) presence of high energy CT transitions, because they would be shadowed by ligand-centred transitions. In this regard, the dotted lines in Figure S9b, located in correspondence of LMCT band onset, are a guide to the eyes to visualize the spectral overlap between the low energy tail of PLE spectra and the high energy tail of LMCT band, that is wider in **4** than in **6**. These overlaps could affect the Eu^{3+} sensitization thus originating the differences between absorption and PLE spectra, and between PLE spectra of compounds **2**, **4** and **6**. The situation is further complicated by the band broadening greatly amplified in the solid state by the presence of strong vibronic interactions that can contribute in mixing the different energy states.

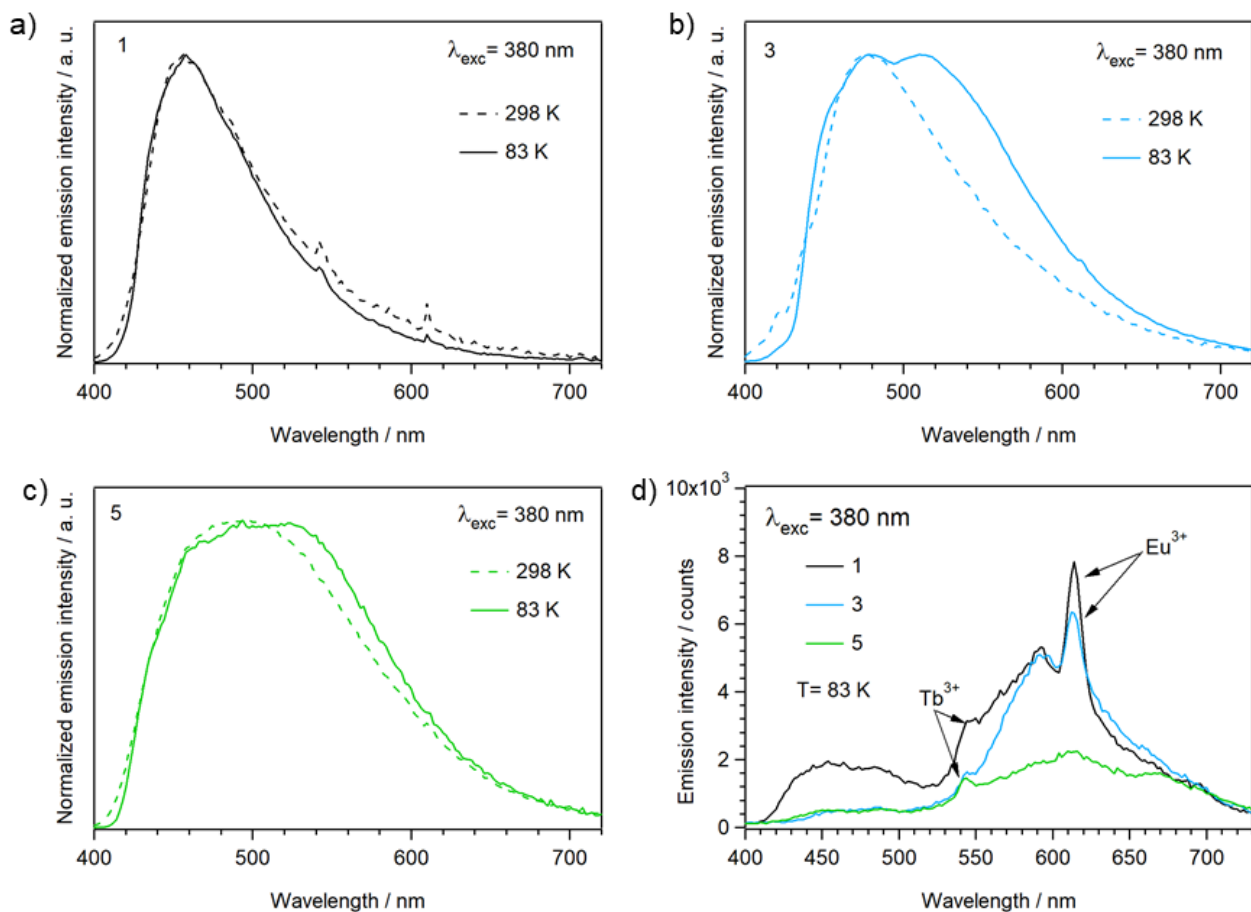


Figure S10. a), b), and c) emission spectra of compounds **1**, **3**, and **5** at 298 K (dashed lines) and 83 K (full lines) temperature. d) Time delayed emission spectra of compounds **1**, **3**, and **5** recorded at 83 K after 40 μ s.

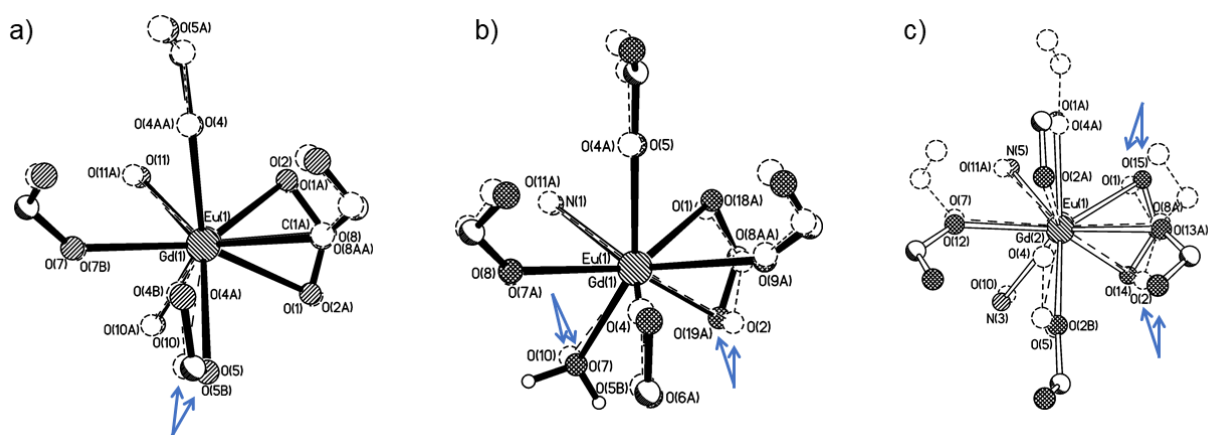


Figure S11. Superimposition of the coordination sphere for: a) **2** and **3**, b) **2** and Gd1 of **5**, c) **2** and Gd2 of **5**.

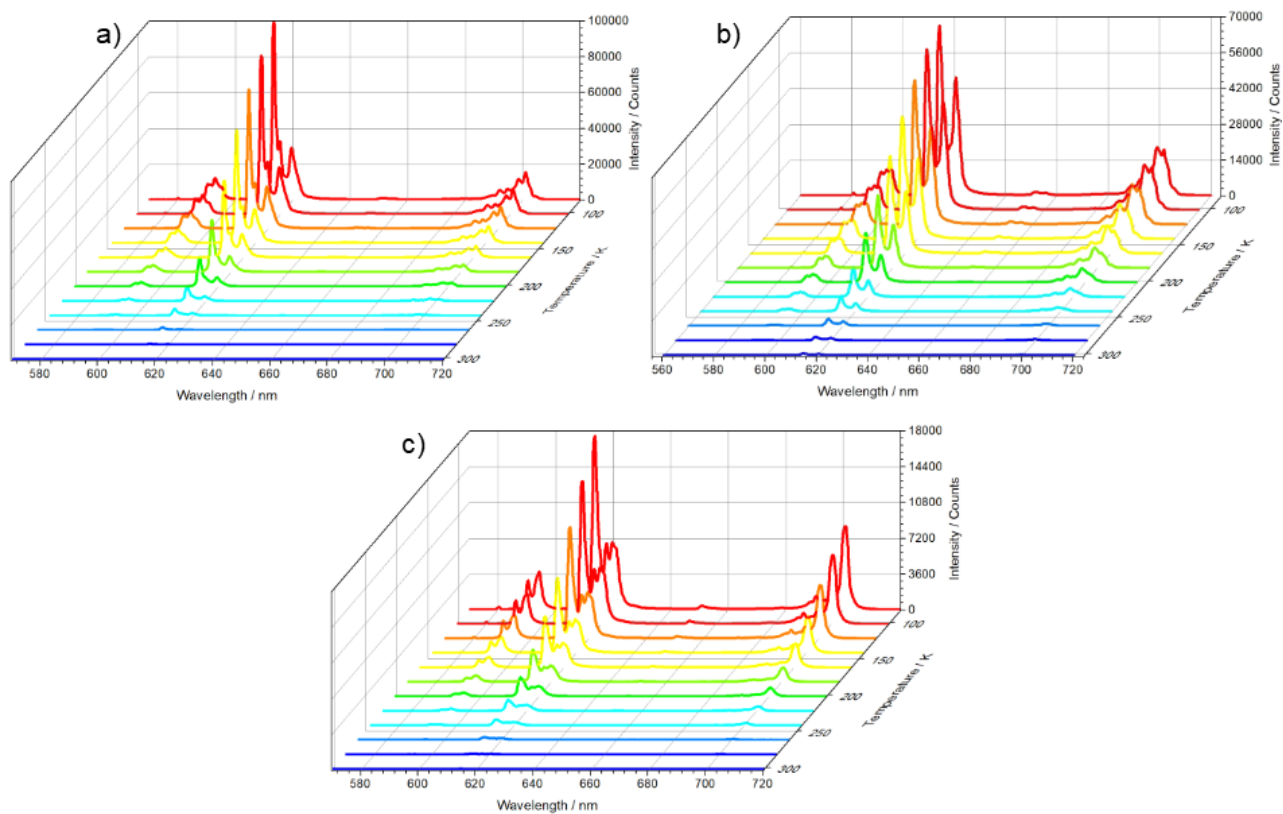


Figure S12. Temperature-dependent emission spectra of compounds **2**, **4**, and **6** in the 83 ÷ 303 K temperature range.

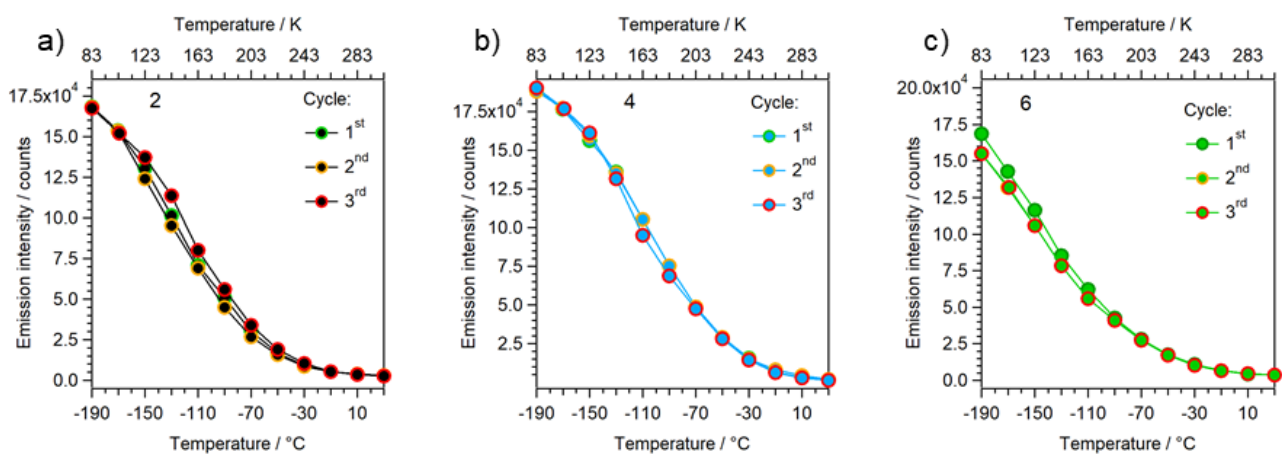


Figure S13. Thermal cycling of compounds a) **2**, b) **4**, and c) **6**.

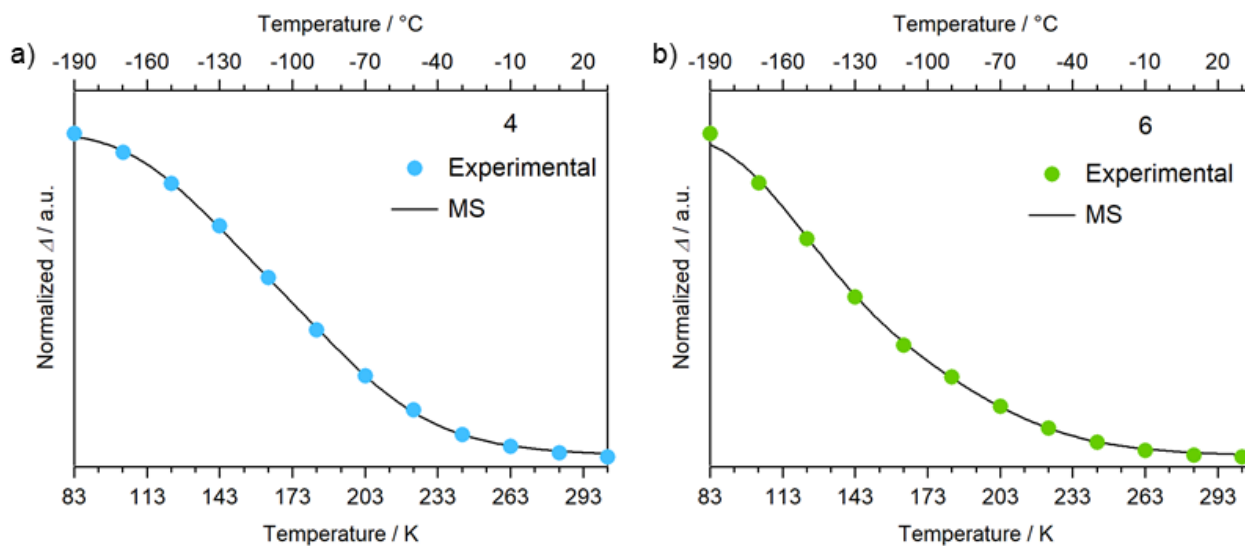


Figure S14. Temperature dependence of the Δ parameter in **4** and **6**. The colored dots represent the experimental points while the black line represents the data of the best fit ($R^2=0.999$) of the Mott-Seitz model (MS) involving two non-radiative recombination channels.

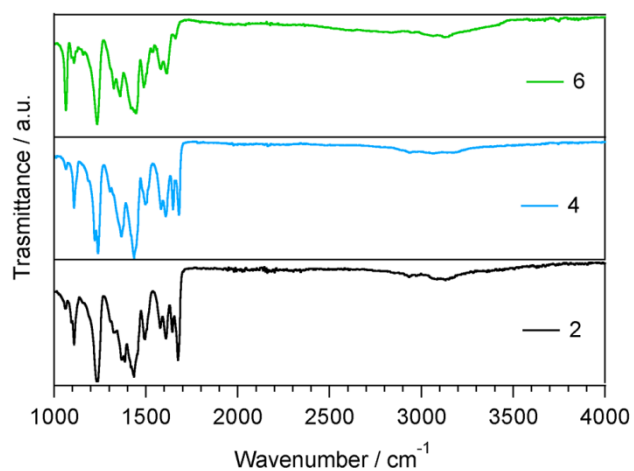


Figure S15. IR spectra of compounds **2**, **4**, and **6**.